Accepted Manuscript

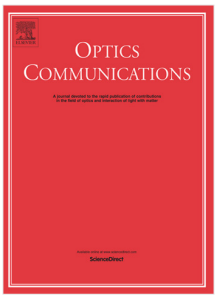

Shared-aperture multifunctional metasurface optical component with low-crosstalk characteristic

Shaowu Wang, Jianjun Lai, Changhong Chen, Xiaoping Li,
Ying Huang, Junqiang Sun

PII: S0030-4018(18)30915-5
DOI: https://doi.org/10.1016/j.optcom.2018.10.040
Reference: OPTICS 23557

To appear in: *Optics Communications*

Received date : 30 July 2018
Revised date : 18 October 2018
Accepted date : 22 October 2018

Please cite this article as: S. Wang, et al., Shared-aperture multifunctional metasurface optical component with low-crosstalk characteristic, *Optics Communications* (2018), https://doi.org/10.1016/j.optcom.2018.10.040

Shared-aperture multifunctional metasurface optical component with low-crosstalk characteristic

Shaowu Wang[1], Jianjun Lai[1, 2, *], Changhong Chen[1], Xiaoping Li[1], Ying Huang[1], and Junqiang Sun[1]

[1]Wuhan National Laboratory for Optoelectronics, Huazhong University of Science & Technology, Wuhan 430074, P. R. China

[2]State Key Laboratory of Applied Optics, Changchun Institute of Optics, Fine Mechanics and Physics, Chinese Academy of Sciences, Changchun 130033, P. R. China

*Corresponding author: Jianjun Lai

Email: jjlai@hust.edu.cn

Abstract

Implementation of multifunctional optical elements by controlling spectrum and wavefront simultaneously with conventional approaches is a difficult task due to their complicated structures and fabrication processes. We present a method to construct multifunctional optical components to achieve independent function at every operating wavelength in a shared-aperture configuration. The component contains amounts of periodical interleaved sectors composed of a metasurface layer sandwiched by two distributed Bragg reflectors (DBRs) and another metasurface layer upon the former. To demonstrate this method, we design and simulate a component which can focus the light wave at 0.521μm on a spot and deflect the wave at 0.581μm to a desired angle. The realized functions for different wavelengths will not interfere with each other, showing a low-crosstalk characteristic. Further improvement is applied to reduce the diffraction effect for light focusing and deflecting with smaller sidelobes by replacing the fixed period of the interleaved sectors with random periods. This work may provide an effective way of controlling the multiwavelength electromagnetic waves in extensive integrated optical systems.

Keywords: metasurfaces, multifunctional component, phase modulation, wavefront control

1. Introduction

Metasurfaces as a new type of optical component to manipulate the electromagnetic wave have attracted more and more attention [1-3]. Compared to conventional bulk optical components relying on the gradual phase accumulation through the electromagnetic wave propagation in the media, metasurfaces consisted of the nanoscale structure array patterned on

a flat surface with special optical properties possess excellent performances and ultrathin thickness. The full control of the amplitudes, phases and polarization states of electromagnetic waves can be achieved. Furthermore, the ultrathin metasurface components can be readily wafer-level manufactured through processes compatible with CMOS technology instead of the traditional machining method for bulk optical components. Such promising approaches prove their great features and functionality, such as polarization control [4-6], holographic images [7-9], beam splitter [10-12], optical focus [13-15] and anomalous refraction [16-18].

Due to the structure and materials dispersion, amounts of the metasurface components were operated at a single wavelength. Multiwavelength control can greatly broaden the application prospect of metasurface, such as achromatic or multifunctional components. Recently, the research work of multiwavelength control became a hotpot, and some wavelength-controlled metasurfaces have been presented [19-30]. Dispersion engineering [19-23] and spatial multiplexing [24-28] are two main approaches to construct the wavelength-controlled metasurfaces. Dispersion engineering is an essentially brute-force search approach by creating the subwavelength-scale building blocks library. Each building block possesses individual multi-wavelength responses. The wavelength-controlled metasurfaces are realized through searching the library and combining the appropriate building blocks with desired responses. However, as the number of functions increases, the construction of metasurface component becomes increasingly difficult, due to the limited design space provided by the building blocks. Spatial multiplexing is a structural segmentation method. In this approach, the metasurface structure is divided into a number of spatial shifters, in which each shifter only effectively acts on one wavelength. Multiwavelength operation is achieved by spatially interleaving phase shifters in the common optical aperture. But this approach also has its intrinsic limitations, such as that the wavelengths crosstalk from adjacent shifters will damage the performance of designed components [23, 25].

In this paper, we present a method or platform to construct wavelength-controlled metasurface component based on the spatial multiplexing. Besides the wavelengths crosstalk limitation of spatial multiplexing can be effectively eliminated. The designed metasurface component possesses low-crosstalk characteristic that the realized functions for different wavelengths will not interfere with each other. The component contains amounts of periodical interleaved sectors, which are divided into different functional regions for the operating wavelengths. Each sector is consisted of two distributed Bragg reflectors as the high reflectivity mirrors and double metasurface layers with different tasks. When the incident wave with broadband or multiwavelength spectrum reaches each sector, it can selectively

transmit through the tunable Fabry-Perot (FP) cavity formed by the two DBR mirrors and a middle metasurface layer. Then the transmitted wave will be further shaped by the top metasurface layer to realize desired phase profile. Finally, the overall phase profiles of the designed functions are obtained through combining the partial phase profiles realized by the sectors. We design and simulate a metasurface component with focusing and deflecting functions at two wavelengths as an example to verify our method. Finally, we further improve the designed component by replacing the fixed period of the interleaved sectors with random periods for achieving a better performance.

2. Principle of multifunctional component design

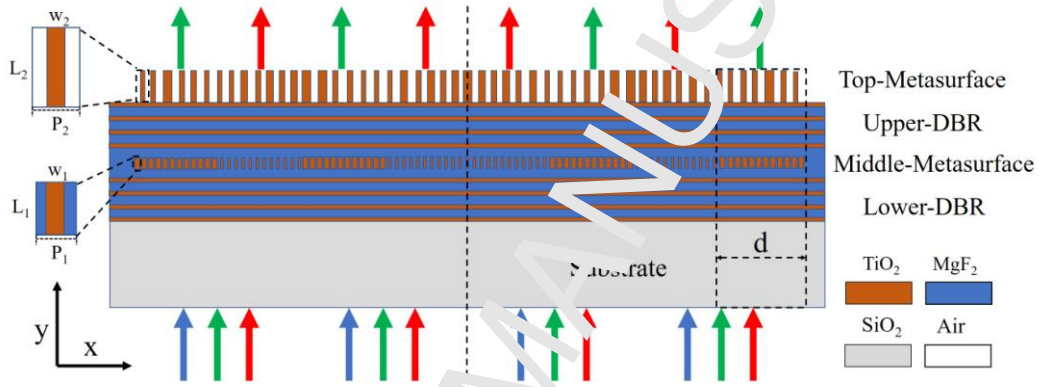

Fig. 1. The schematic representation of shared-aperture multifunctional optical component formed by DBR-metasurface-DBR-metasurface structure.

Figure 1 schematically illustrates the designed shared-aperture multifunctional planar optical component for two wavelengths. The whole structure includes amounts of sectors with fixed period (d) signed in the structural representation and deployed as the interleaved arrangment. The interleaved sectors are divided into different functional regions for corresponding wavelengths and formed by DBR-metasurface-DBR-metasurface structure. According to our design, each sector can perform both filtering and phase manipulation functions. Compared to the metasurface design with composite meta-atom [26], the interleaved sectors can achieve phase manipulation of the wave only at corresponding wavelengths. The DBRs contain 4 pairs of TiO_2 and MgF_2 layers to realize the high reflectivity mirrors. The thicknesses of MgF_2 and TiO_2 layer are $h_1 = 0.1\mu m$ and $h_2 = 0.056\mu m$ respectively according to the formula for the high-reflective film design $h_{1,2} = \lambda_c / 4n_{1,2}$, where $n_1 = 1.38$ and $n_2 = 2.436$ are the refractive indices of MgF_2 and TiO_2 at the central wavelength $\lambda_c = 0.55\mu m$. The dielectric gratings are used to fabricate the double metasurface layers. We choose TiO_2 as the high refractive index grating materials, MgF_2 and air as the low refractive

index insulator materials for middle and top metasurfaces respectively. In our design, the double metasurfaces possess different tasks. The top metasurface layer is designed as the phase shifter to realize wavefront manipulation for each operating wavelength. The middle metasurface, acts as an effective medium layer, is combined with two DBR mirrors to form a tunable FP cavity, which can select the operating wavelengths for the corresponding sectors and prevent the crosstalk between the sectors.

In different grating feature areas, the dielectric grating shows dissimilar physical characteristics. When the period (P) is much smaller than the wavelength of incident light, the dielectric gratings work like a homogeneous dielectric with an effective refractive index according to the principles of effective medium theory (EMT). Furthermore, varying the parameters of the homogeneous dielectric grating (HDG) such as the period, the filling factor and the materials will cause a modulated effective refractive index, as expressed in the formula [31]:

$$n_{TM}^{(2)}=\left\{[n_{TM}^{(0)}]^2+\frac{\pi^2}{3}\left(\frac{P}{\lambda}\right)^2 f^2(1-f)^2(\frac{1}{n_i^2}-\frac{1}{n_s^2})^2[n_{TE}^{(0)}]^2[n_{TM}^{(0)}]^6\right\}^{1/2} \quad (1)$$

Where $n_{TM}^{(2)}$ is the second order approximation of the effective refractive index (n_{eff}) for TM-polarized mode, n_s and n_i are the refractive index of grating and insulator materials. $n_{TE}^{(0)}=\left[(1-f)n_i^2+fn_s^2\right]^{1/2}$ and $n_{TM}^{(0)}=\left[\frac{1-f}{n_i^2}+\frac{f}{n_s^2}\right]^{-1/2}$ are the zeroth order approximation of the effective refractive indices for TE and TM polarized modes respectively. P is the period of grating, and f is the filling factor defined as $f=w/\mathrm{P}$, where w is the width of grating. Therefore, changing the width of grating is seen as an effective approach to manipulate the effective refractive index. In Fig. 2(b), we present the effective refractive index (n_{eff}) of the HDG in the spectral range from $0.5\mu m$ to $0.65\mu m$, with the period $P_1=0.2\mu m$, the height $L_1=0.15\mu m$, the uniform widths $w_1=0\sim0.2\mu m$, and TiO_2 (MgF_2) as the grating (insulator) dielectric. The width w_1 and wavelength λ have the important influence on the effective refractive index, and HDG with varied w_1 and λ will achieve n_{eff} from 1.38 to 2.48. At the same time, figure. 2(c) detailly illustrates the effective refractive indices for the widths $w_1=0.1\mu m$ and $0.16\mu m$ in the spectral range from $0.5\mu m$ to $0.65\mu m$. The HDG possesses the larger effective refractive index for $w_1=0.16\mu m$, and the effective refractive index will decrease with the increase of the wavelength. We can obtain a larger effective refractive index by only increasing the grating width with the other structural parameters unchanged. Therefore, the middle metasurface layer with two DBR mirrors can construct a tunable FP

cavity with varied effective refractive indices by changing the grating widths. The resonance wavelength λ with the maximum transmission rate of FP cavity is able to be described by equation (2):

$$\lambda = \frac{2n_{eff}L_1}{m + (\varphi_1 + \varphi_2)/2\pi} \tag{2}$$

Where φ_1 and φ_2 are the reflection phases generated by the two DBR mirrors, m represents the resonant number. Based on equation (2), the resonance wavelength λ can be controlled by adjusting the effective refractive index, which is related with the grating width. Consequently, we can achieve the required operating wavelengths by selecting appropriate grating widths, such as $w_1 = 0.04\mu m$ for $\lambda = 0.521\mu m$ and $w_1 = 0.16\mu m$ for $\lambda = 0.585\mu m$.

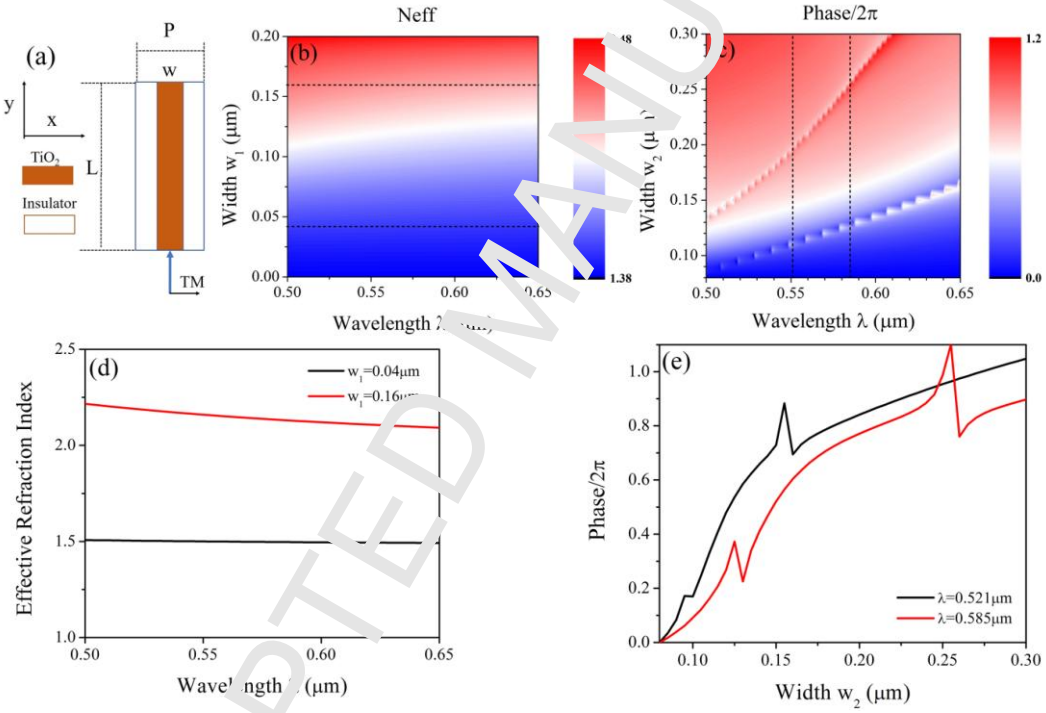

Fig. 2. (a) The schematic of dielectric nano-grating as the unit cell. (b) The effective refractive indices and (c) the phases of the grating array in the spectral range from 0.5μm to 0.65μm, where $P_1 = 0.2\mu m$, $L_1 = 0.15\mu m$, $w_1 = 0 \sim 0.2\mu m$ for the effective refractive index modulation, and $P_2 = 0.45\mu m$, $L_2 = 0.5\mu m$, $w_2 = 0.08 \sim 0.3\mu m$ for the phase modulation. (d) The effective refractive indices of the grating array at different widths $w_1 = 0.04\mu m$ and $w_1 = 0.16\mu m$. (e) The phases of the grating array as the varied widths for different wavelengths $\lambda = 0.521\mu m$ and $\lambda = 0.585\mu m$.

If the dielectric grating with appropriate structural parameters can support internal multiple modes propagation, but prevent external non-zero modes, the so-called resonance phenomenon will arise in it [32]. In this situation, the interaction of wave in the dielectric

grating becomes a complex process and has a high sensitivity to the local geometry. The electromagnetic wave can be manipulated effectively by adjusting the structure parameters of the resonance dielectric grating (RDG). Based on the data obtained from simulation calculation, figure 2(c) presents the phase of the grating array in the spectral range from $0.5\mu m$ to $0.65\mu m$ with fixed period $P_2 = 0.45\mu m$ and height $L_2 = 0.5\mu m$, varied widths $w_2 = 0.08 \sim 0.3\mu m$, and air as the insulator. The coverage of phases will reach 2π in a wide spectral range from $0.5\mu m$ to $0.619\mu m$, which means the wavefront of the outgoing electromagnetic wave in this spectral range can be completely controlled through the gratings with different widths. The relationship between phases and grating widths at two wavelengths $\lambda = 0.521\mu m$ and $0.585\mu m$ are shown in Fig. 2(e). The grating with particular width corresponds to the special phase for each wavelength, which has the overall increase tendency from 0 to 2π as the width varying from $0.08\mu m$ to $0.3\mu m$.

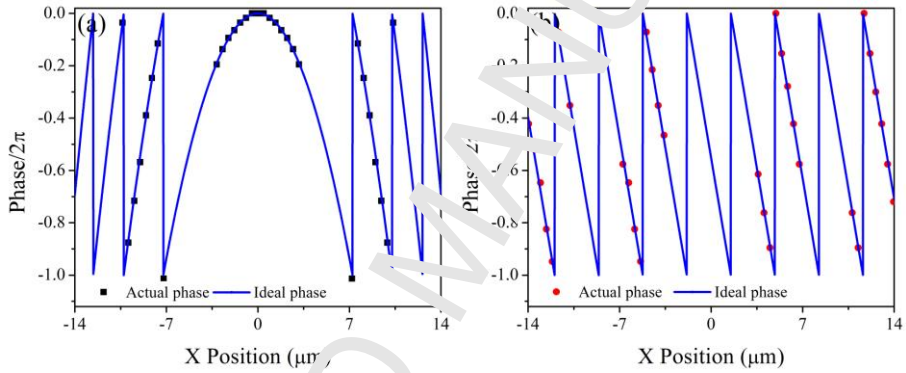

Fig. 3 When the period of the interleaved sectors are fixed at $d = 3.6\mu m$, a part of the desired actual and ideal phase profile distribution along x direction to realize (a) the focusing function for $\lambda = 0.521\mu m$, and (b) the deflecting function for $\lambda = 0.585\mu m$.

The realization of shared-aperture multifunctional planar optical components depends on the wavefront manipulation function of the interleaved sectors. To demonstrate the feasibility of this method, we design and simulate a component with focusing and deflecting functions at two different wavelengths as an example. The aperture of the whole structure is designed as $D = 71.55\mu m$ including 20 interleaved sectors with a fixed period ($d = 3.6\mu m$), which are arranged as centrosymmetric distribution (the symmetrical central nano-gratings are shared by two adjacent sectors). Each sector has 18 and 8 nano-gratings in the middle and top metasurface layers respectively. The whole structure contains two functional regions for the operating wavelengths $\lambda = 0.521\mu m$ and $0.585\mu m$ by deploying the middle HDG array with the widths $w_1 = 0.04\mu m$ and $0.16\mu m$ at the corresponding interleaved sectors. The first functional region is designed as the focusing lens for $\lambda = 0.521\mu m$. The required phase shift distribution of outgoing electromagnetic wave along x direction for realizing focusing

function relies on the phase profile [13]:

$$\Delta\varphi(x) = 2\pi\left(f - \sqrt{f^2 + x^2}\right)/\lambda + 2m\pi \quad (3)$$

Here $f = 50\mu m$ is the focus length, $\lambda = 0.521\mu m$ is the operating wavelength, x is the distance from the center of the lens, and $m = 0, \pm 1, \pm 2\cdots$ represents the girdle number. The phase profile is implemented by choosing the corresponding widths of RDC at each point from Fig. 2(e). Besides, we present a part of the actual phase dispersed distribution and ideal phase profile curve in Fig. 3(a). The actual phase dispersed distribution can fit to the ideal phase curve and support the phase profile of the focusing function. The second functional region is designed as the deflecting refractor for $\lambda = 0.585\mu m$, and the requisite phase profile can be expressed as [19]:

$$\Delta\varphi(x) = -2\pi x\sin(\theta)/\lambda + 2m\pi \quad (4)$$

Where $\theta = 10^0$ is the deflecting angle, $\lambda = 0.585\mu m$ is the operating wavelength, and x is the distance from the left edge of the refractor. We have also plotted a part of the actual phase dispersed distribution and the ideal phase profile curve to achieve the deflecting function in Fig. 3(b). Moreover, the actual dispersed phases for $\lambda = 0.521\mu m$ and $0.585\mu m$ are arranged as the interleaved distribution along x position to implement both focusing and deflecting functions.

3. Simulation of designed component and discussion

The finite-difference time-domain (FDTD) method is adopted as the main way to simulate the proposed device. When the TM-polarized plane electromagnetic wave (along the x direction) is launched normally to the designed structure, only the wave at the resonant wavelengths of the F-P cavity can pass through it. As shown in Fig. 4(a), which is the transmission spectrum response of the designed structure, only two Lorentzian shaped peaks exist at $0.521\mu m$ and $0.585\mu m$ in the spectral range from $0.5\mu m$ to $0.65\mu m$. The transmittances for $\lambda = 0.521\mu m$ and $0.585\mu m$ are about 0.34 and 0.35 respectively, which are not large enough due to only a half of the whole areas for each concerned functional region. But we can adjust the transmittance of emitted wave at the resonant wavelengths by manipulating the proportion of the functional regions in the whole structure. Furthermore, the emitted wave at the resonant wavelength $\lambda = 0.521\mu m$ can be focused on a spot as shown in Fig. 4(b). The focus spot is about $f_t = 51.25\mu m$ away from the central of the middle metasurface layer with a numerical aperture (NA) of 0.58 (the actual focus length is $f = f_t - g = 50.301\mu m$, here $g = 0.949\mu m$ is the distance between the middle and top metasurface layers). In Fig. 4(d), we

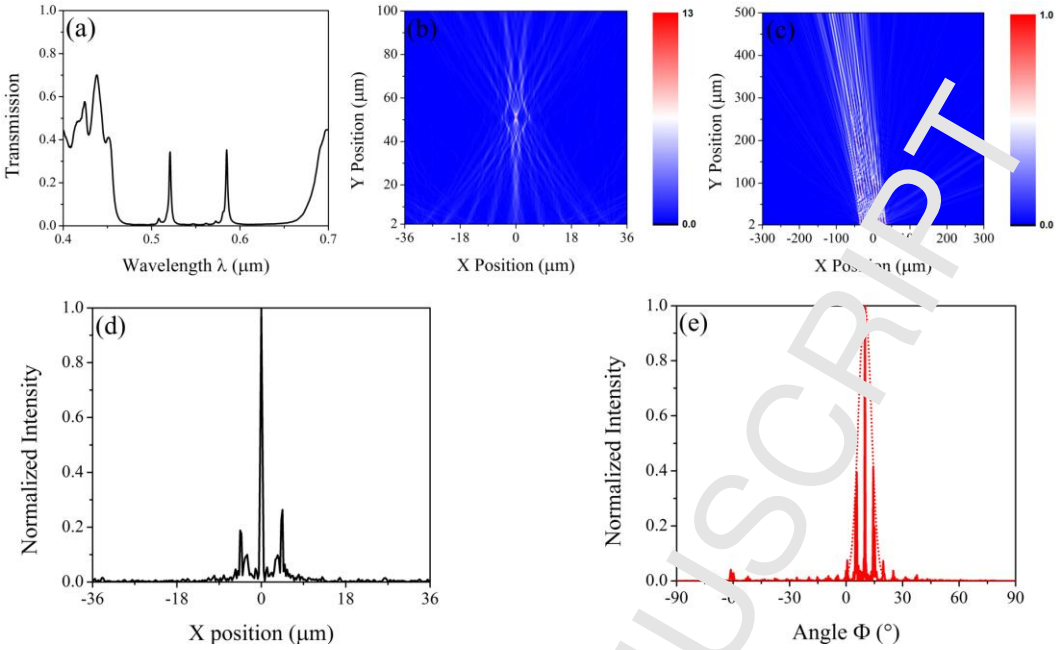

Fig. 4. (a) The transmission spectrum response of the designed structure. When the period of the interleaved sectors are fixed at $d = 3.6\mu m$, the far field intensity distributions for the resonant wavelengths (b) $\lambda = 0.521\mu m$ and (c) $\lambda = 0.585\mu m$. (d) The cross section of the achieved focus spot along x direction for $\lambda = 0.521\mu m$. (e) The far field angular spectrum of the structure as the deflector for $\lambda = 0.585\mu m$.

present the normalized intensity peaks in the cross section of focus spot along x direction. A sharp highest peak exists at the position $x = 0\mu m$, representing most of the wave is focused on the point. The full width at half maximum (FWHM) of the intensity peak is $0.47\mu m$ close to the diffraction limit ($FWHM = 0.51\lambda / NA$). However, there are two lower peaks at $x = \pm 4.5\mu m$, which is the diffraction sidelobes due to the periodical sectors. The efficiency for focusing function is defined as the energy flow ratio of the focal spot area to that passing through the structure for $\lambda = 0.521\mu m$. The energies are achieved through integrating the field intensities of the focal spot and the whole region along x direction respectively, then we will achieve the focusing efficiency $\eta_f = 21.8\%$. Figure 4(c) presents the far field intensity distributions for the resonant wavelengths $\lambda = 0.585\mu m$. The normal incident electromagnetic wave has the anomalous deflection phenomenon. A detailed evaluation of the deflection effect can be obtained through the angular spectrum of the far field in Fig. 4 (e). As expected, the maximum angular spectrum peak is localized at the angle of 10^0. Similarly, according to the integration method, we can obtain the deflecting efficient $\eta_r = 29.6\%$, which is the energy flow ratio of designed deflection angle to that passing through the structure for $\lambda = 0.585\mu m$. Besides two symmetric lower peaks exist on both sides of the highest peak, due to the diffraction effect of the periodical sectors. The deflection angles can be treated as

an envelope as dotted line described in the angular spectrum. Therefore, both the focusing and deflecting functions can be achieved through our designed component. In addition, the focusing and deflecting at two separated resonant wavelengths $\lambda = 0.521\mu m$ and 0.585μm rarely interfere with each other, which represents a low-crosstalk characteristic of the designed component.

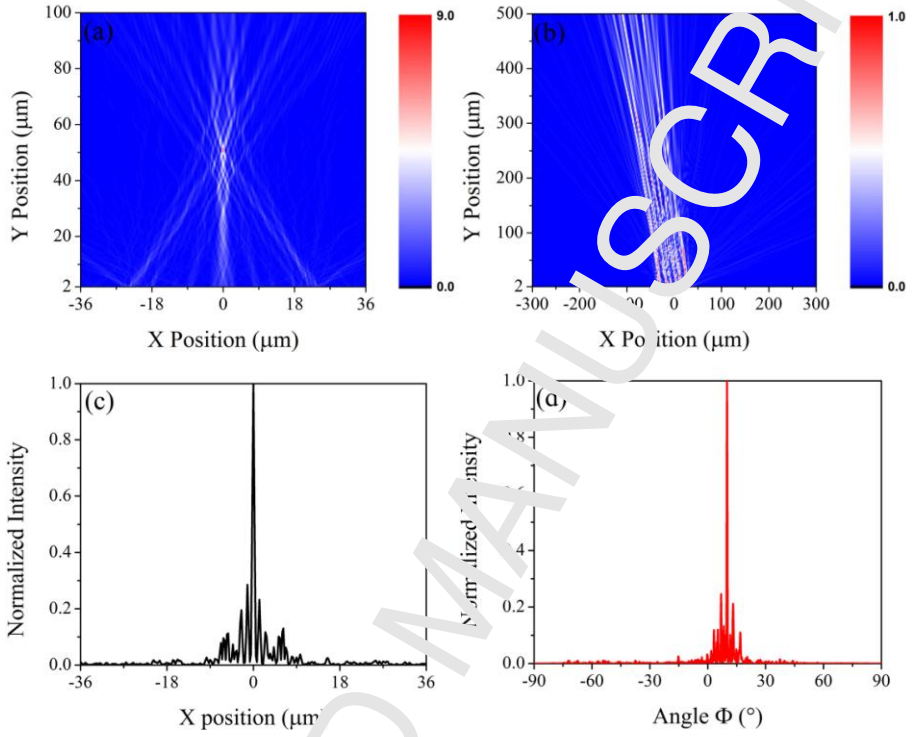

Fig. 5 When the periods of the interleaved sectors are random, the far field intensity distributions of the resonant wavelengths (a) $\lambda = 0.521\mu m$ and (b) $\lambda = 0.585\mu m$. (c) The cross section of the achieved focus spot along x direction for $\lambda = 0.521\mu m$. (d) The far field angular spectrum of the structure as the deflectors for $\lambda = 0.585\mu m$.

The interleaved sectors with fixed period will cause the diffraction sidelobes as shown in Fig. 4(d)(e), which may be detrimental to the performance of the component. It is necessary to optimize the structure to reduce the diffraction effect. The diffraction phenomenon can be effectively reduced by the destruction of periodicity. Then we will replace the fixed period of the interleaved sectors with random periods (the value of period d is non-uniform) for diminishing the diffraction sidelobes. Figure 5(a)(b) present the far field intensity distributions of the component at the resonant wavelengths $\lambda = 0.521\mu m$ and 0.585μm, when the periods of the interleaved sectors are random. The focusing function and the deflecting function can also be realized very well. Corresponding cross section of the focus spot along x direction for $\lambda = 0.521\mu m$ and the far field angular spectrum for $\lambda = 0.585\mu m$ are presented in the Fig. 5(c)(d). The focusing and deflecting efficient can reach $\eta_f = 19.4\%$ and $\eta_r = 26.2\%$.

We can see that the field intensity value of diffraction sidelobes is reduced, and the contrast between the main peaks and the diffraction peaks is improved obviously. Therefore, the diffraction effect is suppressed effectively.

As a final remark, it is noteworthy that there are some practical routes to fabricate the component depicted above. Next, we will show one route here as an example. The wavelength-controlled metasurface component can be implemented on a silicon dioxide (SiO_2) substrate by modern nanofabrication and deposition technology. Firstly, we can choose electron beam evaporation (EBE) to deposit the lower-DBR layer formed by 4 pairs of TiO_2 and MgF_2 layers. Then on the DBR layer, the nano-grating patterns of the middle metasurface layer will be defined by electron beam lithography (EBL) and lift-off techniques [33, 34]. Next MgF_2 is deposited to fill the gaps between nano-grating and planarized by chemically mechanical polishing (CMP) [35]. Through the similar processes, we can obtain the upper-DBR layer and top metasurface layer.

4. Conclusion

In summary, we present an approach to achieve shared-aperture multifunctional optical component with low-crosstalk characteristic based on DBR-metasurface-DBR-metasurface structure. Research results indicate that the middle metasurface with two DBRs work as a tunable FP cavity and the top metasurface layer can control the wavefront of outgoing electromagnetic wave. The wave at desired wavelengths can be selected through the tunable FP cavity and manipulated by the top metasurface layer. A metasurface component composed by the amounts of the interleaved sectors with fixed period is exhibited. Through simulation calculation, the electromagnetic wave at the resonant wavelength $\lambda = 0.521\mu m$ can be focused on a spot ($f_t = 51.25\mu m$) by the designed component, while it can also deflect the wave at $\lambda = 0.585\mu m$ to the desired angle ($\theta = 10^0$). Furthermore, the realized focusing and deflecting functions will not interfere with each other. Therefore, the designed component can realize multiple functions and possesses low-crosstalk characteristic. For better performance, we have improved the design to suppress the diffraction effect for light focusing and deflecting with smaller sidelobes by replacing the fixed period of the interleaved sectors with random periods. This work provides an effective solution for achieving wavelength-controlled metasurface, which may have the potential applications in integrated optical systems.

Acknowledgments

This work was supported by the National Natural Science Foundation of China (NSFC) (61474051), the Fundamental Research Funds for the Central Universities (HUST:

2016YXMS022) and the State Key Laboratory of Applied Optics.

References

1. N. F. Yu, P. Genevet, M. A. Kats, F. Aieta, J. P. Tetienne, F. Capasso, and Z. Gaburro, "Light Propagation with Phase Discontinuities: Generalized Laws of Reflection and Refraction," Science 334 (6054), 333-337 (2011).
2. D. M. Lin, P. Y. Fan, E. Hasman, and M. L. Brongersma, "Dielectric gradient metasurface optical elements," Science 345 (6194), 298-302 (2014).
3. N. Yu, and F. Capasso, "Flat optics with designer metasurfaces," Nat. Mater. 13 (2), 139-150 (2014).
4. J. Lin, J. P. B. Mueller, Q. Wang, G. H. Yuan, N. Antoniou, X. C. Yuan, and F. Capasso, "Polarization-controlled tunable directional coupling of surface plasmon polaritons," Science 340 (6130), 331-334 (2013).
5. N. Yu, F. Aieta, P. Genevet, M. A. Kats, Z. Gaburro, and F. Capasso, "A broadband, background-free quarter-wave plate based on plasmonic metasurfaces," Nano Lett. 12 (12), 6328-6333 (2012).
6. N. K. Grady, J. E. Heyes, D. R. Chowdhury, Y. Zeng, M. T. Reiten, A. K. Azad, A. J. Taylor, D. A. R. Dalvit, and H. T. Chen, "Terahertz Metamaterials for Linear Polarization Conversion and Anomalous Refraction," Science 340, 1304-1307 (2013).
7. L. L. Huang, X. Z. Chen, H. Mühlenbernd, H. Zhang, S. M. Chen, B. F. Bai, Q. F. Tan, G. F. Jin, K. W. Cheah, C. W. Qiu, J. S. Li, T. Zentgraf, and S. Zhang, "Three-dimensional optical holography using a plasmonic metasurface," Nat. Commun. 4, 2808 (2013).
8. Z. L. Deng, S. Zhang, G. P. Wang, "A facile grating approach towards broadband, wide-angle and high-efficiency holographic metasurfaces," Nanoscale 8 (3), 1588-1594 (2016).
9. G. X. Zheng, H. Muhlenbernd, M. Kenney, G. X. Li, T. Zentgraf, and S. Zhang, "Metasurface holograms reaching 80% efficiency," Nat. Nanotechnol. 10 (4), 308-312 (2015).
10. M. Khorasaninejad, and K. B. Crozier, "Silicon nanofin grating as a miniature chirality-distinguishing beam-splitter," Nat. Commun. 5, 5386 (2014).
11. M. Khorasaninejad, W. Zhu, and K. B. Crozier, "Efficient polarization beam splitter pixel based on a dielectric metasurface," Optica 2 (4), 376-382 (2015).
12. Q. Zhang, Li M, T. Liao, and X. Cui, "Design of beam deflector, splitters, wave plates and metalens using photonic elements with dielectric metasurface," Opt. Commun. 411, 93-100 (2018).

13. M. Khorasaninejad, W. T. Chen, R. C. Devlin, J. Oh, A.Y. Zhu, and F. Capasso, "Metalenses at visible wavelengths: Diffraction-limited focusing and subwavelength resolution imaging," Science 352 (6290), 1190-1194 (2016)
14. M. Khorasaninejad, A. Y. Zhuit, C. Roques-Carmes, W. T. Chen, J. Oh, I. Mishra, R. C. Devlin, and F. Capasso, "Polarization-Insensitive Metalenses at Visible Wavelengths," Nano Lett. 16 (11), 7229-7234 (2016).
15. A. Özdemir , Z. Hayran, Y. Takashima, and H. Kurt, "Polarization independent high transmission large numerical aperture laser beam focusing and deflection by dielectric Huygens' metasurfaces," Opt. Commun. 401, 46-53 (2017)
16. L. L. Huang, X. Z. Chen, H. Muhlenbernd, G. X. Li, B. F. Bai, Q. F. Tan, G. F. Jin, T. Zentgraf, and S. Zhang, "Dispersionless Phase Discontinuities for Controlling Light Propagation," Nano Lett. 12 (11), 5750-5755 (2012).
17. Z. Wang, S. He, Q Liu, and W. Wang, "Visible light metasurfaces based on gallium nitride high contrast gratings," Opt. Commun 367, 144-148 (2016) .
18. H. Yang, and Y. Deng, "Broadband and high efficiency all-dielectric metasurfaces for wavefront steering with easily obtained phase shift," Opt. Commun. 405, 39-42 (2017).
19. F. Aieta, M. A. Kats, P. Genevet, and F. Capasso, "Multiwavelength achromatic metasurfaces by dispersive phase compensation," Science 347 (6228), 1342-1345 (2015).
20. M. Khorasaninejad, F. Aieta, P. Kanhaiya, M. A. Kats, P. Genevet, D. Rousso, and F. Capasso, "Achromatic Metasurface Lens at Telecommunication Wavelengths," Nano Lett. 15 (8), 5358-5362 (2015).
21. M. Khorasaninejad, Z. Shi, A. Y. Zhu, W. T. Chen, V. Sanjeev, A. Zaidi, and F. Capasso, "Achromatic Metalens over 60 nm Bandwidth in the Visible and Metalens with Reverse Chromatic Dispersion," Nano Lett. 17 (3): 1819-1824 (2017).
22. E. Arbabi, A. Arbabi, S. M. Kamali, Y. Horie, and A. Faraon, "Controlling the sign of chromatic dispersion in diffractive optics with dielectric metasurfaces," Optica 4 (6), 625-632 (2017).
23. Z. Shi, M. Khorasaninejad, Y. W. Huang, C. R. Carmes, A. Y. Zhu, W. T. Chen, V. Sanjeev, Z. W. Ding, M. Tamagnone, K. Chaudhary, R. C. Devlin, C. W. Qiu, and F. Capasso. "Single-Layer Metasurface with Controllable Multiwavelength Functions," Nano lett. 18 (4), 2420-2427 (2018).
24. E. Arbabi, A. Arbabi, S. M. Kamali, Y. Horie, and A. Faraon, "Multiwavelength metasurfaces through spatial multiplexing," Sci. Rep. 6, 32803 (2016).
25. J. Hu, C. H. Liu, X. Ren, L. J. Lauhon, and T. W. Odom, "Plasmonic Lattice Lenses for Multiwavelength Achromatic Focusing," ACS Nano 10 (11), 10275-10282 (2016).

26. J. Ding, S. An, B. Zheng, and H. Zhang, "Multiwavelength Metasurfaces Based on Single -Layer Dual-Wavelength Meta-Atoms: Toward Complete Phase and Amplitude Modulations at Two Wavelengths," Adv. Optical Mater. 5 (10), 1700079 (2017).
27. J. Ding, N. N. Xu, H. Ren, Y. K. Lin, W. L. Zhang, and H. L. Zhang, "Dual-Wavelength Terahertz Metasurfaces with Independent Phase and Amplitude Control at Each Wavelength," Sci. Rep. 6, 34020 (2016).
28. D. Sell, J. Yang, S. Doshay, and J. A. Fan, "Periodic Dielectric Metasurfaces with High- Efficiency, Multiwavelength Functionalities," Adv. Optical Mater. 5 (23), 1700645 (2017).
29. S. Wang, J. Lai, T. Wu, X. Li, and J. Su, "Wide-band achromatic metalens for visible light by dispersion compensation method," J. Phys. D: Appl. Phys. 50 (45), 455101(2017).
30. Z. L. Deng, S. Zhang, and G. P. Wang, "Wide-angled off-axis achromatic metasurfaces for visible light," Opt. Express 24 (20), 23118-23128 (2016).
31. D. H. Raguin, and G. M. Morris, "Analysis of antireflection-structured surfaces with continuous one-dimensional surface profiles," Appl. Opt. 32 (14), 2582-2598 (1993).
32. S. Vo, D. Fattal, W. V. Sorin, Z. Peng, T. Tran, M. Fiorentino, and R. G. Beausoleil, "Sub-wavelength grating lenses with a twist," IEEE Photonics Technol. Lett. 26 (13), 1375-1378 (2014).
33. Y. Horie, A. Arbabi, E. Arbabi, S. M. Kamali, and A. Faraon, "Wide bandwidth and high resolution planar filter array based on DBR-metasurface-DBR structures," Opt. Express, 24 (11), 11677-11682 (2016).
34. A. Arbabi, E. Arbabi, S. M. Kamali, Y. Horie, S. Han, and A. Faraon, "Miniature optical planar camera based on a wide-angle metasurface doublet corrected for monochromatic aberrations," Nat. Commun. 7, 13682 (2016).
35. P. B. Zantye, A. Kumar, A. K.Sikder, "Chemical mechanical planarization for microelectronics applications," Mater. Sci. Eng. R, 45 (3-6), 89-220 (2004).